Kalman Filter Based State Estimation for MAVs

Mehmet Direktaş*, Göktuğ M. Kesici†, Tunahan Aslan‡, and Berkay F. Doğan§
Middle East Technical University, Ankara, Çankaya, 06800, Turkey

Navigation is one of the most fundamental problems of a flying object, and in this report, the position, velocity, and attitude of a drone in an indoor environment will be estimated. In order to achieve this task, the gyroscopes and accelerometers are used for the dead reckoning system while the 7 UWB (Ultra Wide Band) anchors are used for external information. The motion of the drone is a simple square trajectory and it moves for a small distance. Due to the non-linearities that have been analyzed in the system EKF (Extended Kalman Filter) which is a special type of Kalman Filter will be used in order to merge the information that comes from both UWB and IMU (Inertial Measurement Unit) measurements. After that, to have a better result, a second external information source will be used which is VIO (Visual Inertial Odometry), and it will be shown that by using another external source, the result is improved.

I. Nomenclature

B	=	UWB biases $[b_1, b_2, .., b_6, b_7]^T$
DCM	=	direction cosine matrix
EKF	=	extended kalman filter
ENU	=	east north up
GNSS	=	global navigation satellite system
IMU	=	inertial measurement unit
MAV	=	micro air vehicle
P	=	position of the drone $[x, y, z]^T$
Q	=	attitude of the drone $[q_1, q_2, q_3, q_4]^T$
UWB	=	ultra-wideband sensors
V	=	velocity of the drone $[v_x, v_y, v_z]^T$
VIO	=	visual-inertial odometry

II. Introduction

After the first serious analysis of MAV at Naval Research Laboratory [1], it became more and more popular in the late '90s. Today, they are used in various applications such as the logistics industry. [2]. Therefore, it is important to analyze them closely and examine their effectiveness for crucial operations. In this report, the navigation problem of a drone will be considered. The position, velocity, and attitude of the drone will be tried to estimate. In order to achieve this task, real flight test data is taken from TUM (Technical University of Munich) [3]. The maneuver that has been analyzed is in an indoor environment where GNSS is not available. Therefore, as an external source, 7 UWB (Ultra Wide Band) anchors which are DW100-base Bitcraze Loco Positioning ultrawideband radios are used to have range measurements. Unfortunately, the gyroscope and accelerometer are not specified in the dataset. Yet the dataset is valuable enough because it contains ground truth data from Leica Total station and Visual Inertial Odometry which is Intel Realsense T265/T261 tracking camera. For both ground truth and VIO data, the position and orientation of the drone are given. The first problem that is been encountered during this project is that measurements from IMU and UWB anchors were not synchronized. Therefore, linear interpolation was applied. Moreover, the sampling time of both IMU and UWB anchors is changed so that we have IMU measurements obtained at 100 Hz and the UWB anchors measurements at 3 Hz. The motion of the drone is not a complicated one. It vertically ascends on a straight path, and makes a simple square trajectory at the constant altitude; then, descends on a straight path again.

*Undergraduate Student, Aerospace Engineering
†Undergraduate Student, Aerospace Engineering
‡Undergraduate Student, Aerospace Engineering
§Undergraduate Student, Aerospace Engineering

III. Related Work

With the increasing popularity of the MAVs, various state estimation algorithms have been proposed. The tightly coupled [4], and loosely coupled [5] implementations have been shown previously for the range-based sensors. In problems where multiple sensors are available, the data fusion techniques with parametric methods [5, 6], and non-parametric methods [7] are proposed. Recently, with the advent of learning-based computer vision algorithms, the vision-based approaches also gained traction. Some researchers suggested the absolute position and the orientation of the drone can be obtained by detecting certain features. By fusing the data coming from the camera with the IMU, UWB, or VIO measurements, accurate estimations can be obtained [8, 9]. However, one drawback of these methods is they are computationally expensive; hence, those algorithms are not feasible to implement on small platforms like ours.

IV. Methodology

A. Assumptions

In order to make the problem simpler, some assumptions have been made. For instance, we assumed that the earth was non-rotating, flat and took the ENU (East North Up) as an inertial frame. These are quite fair assumptions because the navigation problem that has been analyzed in this report is for an almost 2-meter square trajectory and the duration of the flight is around 50 seconds.

B. Mechanization Equations

The state vector consists of position, velocity, quatrains, and UWB biases as shown in Eq.1. The first step is to write down the Mechanization Equations so that the state space matrix can be obtained.

$$X = \begin{bmatrix} P & V & Q & B \end{bmatrix}^T \tag{1}$$

The derivative of the position is equal to the velocity as shown below, and the relation is linear.

$$\dot{P} = V \tag{2}$$

For the derivative of the velocity terms, the DCM matrix shall be obtained as a function of quaternions first. Then, transforming the specific forces from the body frame to the ENU frame and adding the gravity yields the nonlinear relation formulated below. To use it in the filter, we linearize this equation by taking the Jacobian of accelerations with respect to the quaternion terms, and we call it J_1.

$$\dot{V} = R_{bi}^T f - g \tag{3}$$

$$\dot{V} = \begin{bmatrix} q_1^2 - q_2^2 - q_3^2 + q_4^2 & 2(q_1q_2 + q_3q_4) & 2(q_1q_3 - q_2q_4) \\ 2(q_1q_2 - q_3q_4) & -q_1^2 + q_2^2 - q_3^2 + q_4^2 & 2(q_2q_3 + q_1q_4) \\ 2(q_1q_3 + q_2q_4) & 2(q_2q_3 - q_1q_4) & -q_1^2 - q_2^2 + q_3^2 + q_4^2 \end{bmatrix}^T f - g \tag{4}$$

$$J_1 = \begin{bmatrix} 2(q_1f_x + q_2f_y + q_3f_z) & 2(-q_2f_x + q_1f_y + q_4f_z) & 2(-q_3f_x - q_4f_y + q_1f_z) & 2(q_4f_x - q_3f_y + q_2f_z) \\ 2(q_2f_x - q_1f_y - q_4f_z) & 2(q_1f_x + q_2f_y + q_3f_z) & 2(q_4f_x - q_3f_y + q_2f_z) & 2(q_3f_x + q_4f_y - q_1f_z) \\ 2(q_3f_x + q_4f_y - q_1f_z) & 2(-q_4f_x + q_3f_y - q_2f_z) & 2(q_1f_x + q_2f_y + q_3f_z) & 2(-q_2f_x + q_1f_y + q_4f_z) \end{bmatrix} \tag{5}$$

The next step is to calculate the derivative of the quaternion terms, and it is directly obtained from the quaternion kinematics equation as shown below. Since the angular velocities are not one of the terms of the state matrix, the relation is linear, and we assign that matrix to J_2.

$$\dot{Q} = \frac{1}{2}\Omega(\omega)\, q = \frac{1}{2}\begin{bmatrix} 0 & -\omega_3 & -\omega_2 & \omega_1 \\ -\omega_3 & 0 & \omega_1 & \omega_2 \\ \omega_2 & -\omega_1 & 0 & \omega_3 \\ -\omega_1 & -\omega_2 & -\omega_3 & 0 \end{bmatrix}\begin{bmatrix} q_1 \\ q_2 \\ q_3 \\ q_4 \end{bmatrix} \tag{6}$$

$$J_2 = \frac{1}{2}\begin{bmatrix} 0 & -\omega_3 & -\omega_2 & \omega_1 \\ -\omega_3 & 0 & \omega_1 & \omega_2 \\ \omega_2 & -\omega_1 & 0 & \omega_3 \\ -\omega_1 & -\omega_2 & -\omega_3 & 0 \end{bmatrix} \tag{7}$$

Finally, we assumed the UWB biases are constant; in other words, their derivatives are all zero.

$$\dot{B} = 0 \tag{8}$$

Inserting everything into the below state space form yields a linearized model of our system in the continuous domain.

$$\begin{bmatrix} \dot{P} \\ \dot{V} \\ \dot{Q} \\ \dot{B} \end{bmatrix} = \begin{bmatrix} 0_{3\times3} & 1_{3\times3} & 0_{3\times4} & 0_{3\times7} \\ 0_{3\times3} & 0_{3\times3} & J_{1_{3\times4}} & 0_{3\times7} \\ 0_{4\times3} & 0_{4\times3} & J_{2_{4\times4}} & 0_{3\times7} \\ 0_{7\times3} & 0_{7\times3} & 0_{7\times4} & 0_{7\times7} \end{bmatrix}\begin{bmatrix} P \\ V \\ Q \\ B \end{bmatrix} \tag{9}$$

Since the filter we implement works in the discrete domain, the state space model is discretized using 10.

$$F = e^{A\Delta t} \tag{10}$$

where,

$$A = \begin{bmatrix} 0_{3\times3} & 1_{3\times3} & 0_{3\times4} & 0_{3\times7} \\ 0_{3\times3} & 0_{3\times3} & J_{1_{3\times4}} & 0_{3\times7} \\ 0_{4\times3} & 0_{4\times3} & J_{2_{4\times4}} & 0_{3\times7} \\ 0_{7\times3} & 0_{7\times3} & 0_{7\times4} & 0_{7\times7} \end{bmatrix}, \quad \Delta t = 0.01\ s \tag{11}$$

C. Measurement Model

To develop an integrated navigation solution, there needs to be an external measurement source. UWB and VIO measurements are integrated with INS solutions, as previously mentioned. While position and orientation (4 quaternion terms) are the outputs of the VIO measurements, range measurements are the outputs of the UWB signals. These measurements is updated in every $dt = 0.3s$. The system has seven VIO and seven UWB measurements in total. Three measurements are used by the VIO to determine the drone's position, and four measurements are used to determine its orientation. It is significant to remember that there is a nonlinear relationship between the range measurements and the states (position). The range equation provides this relation. As can be observed in Equation 26, bias is also present in the measurements. These bias terms for each UWB measurement should be estimated.

$$\rho = \sqrt{(x_{uwb} - x_d)^2 + (y_{uwb} - y_d)^2 + (z_{uwb} - z_d)^2} + b \tag{12}$$

In contrast to range measurements, there is a linear relation between the VIO measurements and states (position and orientation). Therefore, the measurement matrix H can be constructed by taking partial derivatives of each measurement with respect to states. There are three states for position, three states for velocity, four states for orientation (quaternions),

and seven states for UWB biases in the model. Since the system has 14 measurements and 17 states, the size of the H matrix is 14x17. These states consist of 3 positions, 3 velocities, 4 quaternions, and 7 UWB biases.

$$H = \begin{bmatrix} \frac{\hat{x}-x_1}{\rho_1} & \frac{\hat{y}-y_1}{\rho_1} & \frac{\hat{z}-z_1}{\rho_1} & & \\ . & . & . & & \\ . & . & . & 0_{7\times7} & I_{7\times7} \\ . & . & . & & \\ \frac{\hat{x}-x_7}{\rho_7} & \frac{\hat{y}-y_7}{\rho_7} & \frac{\hat{z}-z_7}{\rho_7} & & \\ I_{3\times3} & & & 0_{3\times14} & \\ 0_{4\times6} & I_{4\times4} & & & 0_{4\times7} \end{bmatrix} \tag{13}$$

The measurement matrix H relates measurements to states. Also, it is important to note that there is a mismatch between the camera and the body frame. The position error due to mismatching is given in the dataset and coded as Δp_{vio} in the script. This position mismatch error is subtracted from VIO position estimations before the filter.

$$\Delta p_{VIO} = \begin{bmatrix} 0.02 & 0.01 & -0.035 \end{bmatrix}^T \tag{14}$$

To estimate the orientation error due to mismatching, the first orientation data from the ground truth and VIO are used. To find it, quaternion multiplication is applied.

$$\Delta q_{VIO} = q_{VIO_1}^{-1} \otimes q_{GT_1} \tag{15}$$

Normally, ground truth data should not be used for the calculations; however, the difference between the body and the camera frame orientation is not provided. Therefore, that difference is calculated using only the initial attitudes coming from VIO sensor and the ground true data for once, and the same Δq_{VIO} is used for the rest of the measurements. Corrected orientation can be computed by multiplying the orientation measurements that come from the VIO data by the error quaternion calculated by Equation 15. This process is applied in the measurements (z variable in the code). In the end, measurement array z is made up of three corrected position measurements, four corrected quaternion measurements from the VIO data, and seven corrected UWB measurements (estimated bias terms are subtracted).

D. Kalman Filter

The Kalman Filter algorithm is used to integrate the INS solution and external measurements appropriately. As described in the 'Measurement Model' section, there is a nonlinear relationship between the states and the measurements for UWB signals. Also, the prediction part of the filter is nonlinear. In such a case, the use of the Extended Kalman Filter algorithm is more suitable. Initial states and covariance matrices are required to initialize the filter. The Q matrix is the process covariance matrix, which shows the reliability of our mathematical model (process), whereas the P matrix is the state covariance matrix, which shows the reliability of each state. As mentioned before, the system has 17 states, and the initial states are given in Equation 16. The initial state covariance matrix P is determined using engineering judgment. Since velocity and orientation are more reliable than position estimation, their covariances are selected less. The Q and R matrices are constructed using the sensor specifications. Since VIO specifications are not exactly known,

its covariance in Q and R matrices is found by trial and error.

$$X_0 = \begin{bmatrix} 0_{3\times1} & 0_{3\times1} & I_q & 0_{7\times1} \end{bmatrix}^T \tag{16}$$

$$P_{0,pos} = 0.1m \tag{17}$$

$$P_{0,vel} = 0.1m/s \tag{18}$$

$$P_{0,quat} = 0.02 \tag{19}$$

$$P_{0,bias} = 0.1\ m \tag{20}$$

$$P_0 = blkdiag\left(eye\,(3) \times P_{0,pos},\ eye\,(3) \times P_{0,vel},\ eye\,(4) \times P_{0,quat},\ eye\,(7) \times P_{0,bias}\right) \tag{21}$$

$$Q = blkdiag\left(eye\,(3) \times \left(\sigma_{acc}\Delta t^2\right)^2, eye\,(3) \times (\sigma_{acc}\Delta t)^2, eye\,(4) \times 10^{-7}, eye\,(7) \times 10^{-10}\right) \tag{22}$$

$$R = blkdiag\left(eye\,(7) \times \sigma^2{}_{UWB}, eye\,(3) \times 0.1, eye\,(4) \times 0.01\right) \tag{23}$$

$$\sigma_{acc} = 9 \times 10^{-8} m/s^2,\ \ \sigma_{UWB} = 10^{-2} m,\ \ \Delta t = 0.01\ s \tag{24}$$

$$\tag{25}$$

The prediction part of the Kalman filter uses these initial states and covariances. Corresponding equations are given in Equation 28 and Equation 29. The f relation given in the Equation 28 is nonlinear state transition. These state and covariance predictions have not been updated by the measurements yet. Since the measurement frequency is 3 Hz, these predictions are updated three times in a second. The updating equations of Kalman Filter are given in Equation 30, Equation 31,Equation 32. The h relation given in Equation 31, is the predicted range, position, and orientation measurements using predicted states.

$$\rho = \sqrt{(x_{uwb} - x^-)^2 + (y_{uwb} - y^-)^2 + (z_{uwb} - z^-)^2} \tag{26}$$

$$h = \begin{bmatrix} \rho^-_{1:7} & x^- & y^- & z^- & q^-_1 & q^-_2 & q^-_3 & q^-_4 \end{bmatrix}^T \tag{27}$$

Since the frequency of the INS solution is 100 Hz, there is no available measurement for every time step. In these instances, updated state and covariance estimations become equal to the predicted ones. In other words, Kalman gain (K) becomes equal to zero.

$$x^-_{k+1} = f\,(x_k) \tag{28}$$

$$P^-_{k+1} = FP_kF^T + Q \tag{29}$$

$$K = P^-_{k+1}H^\top (HP^-_{k+1}H^\top + R)^{-1} \tag{30}$$

$$x^+_{k+1} = x^-_{k+1} + K(z - h(x^-_{k+1})) \tag{31}$$

$$P^+_{k+1} = (I_{17\times17} - KH)P^-_{k+1} \tag{32}$$

Outputs of the Kalman filter are corrected states and state covariances. The results will be discussed in the 'Results' section.

V. Results

Three different navigation solutions are implemented and analyzed throughout the project. The first one is the Inertial navigation system case, which purely depends on the inertial measurement unit sensors, gyroscope, and accelerometer. The second one is INS and UWB measurements, which are external measurements that update the estimation. In the last case, instead of one, two external measurements are considered together, which are UWB and VIO.

The results of the INS-only case are plotted below in Figures 1 to 7 as follows.

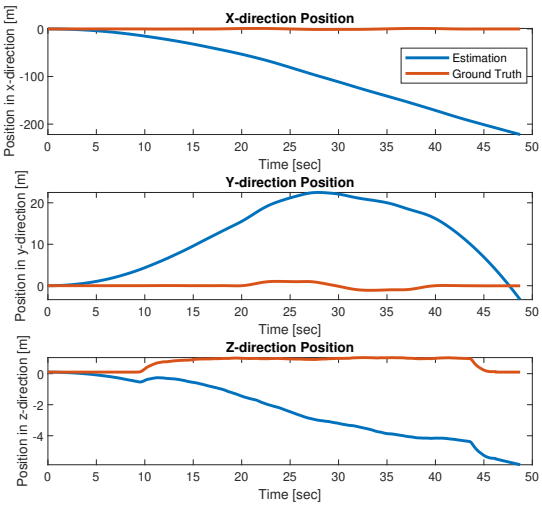

Fig. 1 INS only case position estimations.

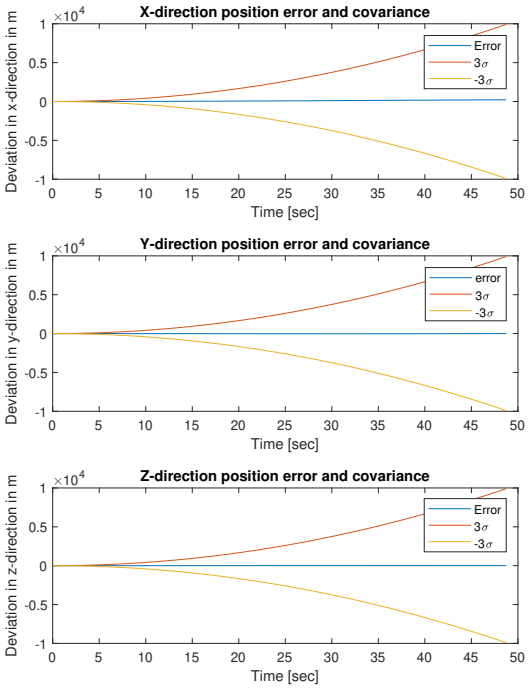

Fig. 2 INS only case position estimation covariances.

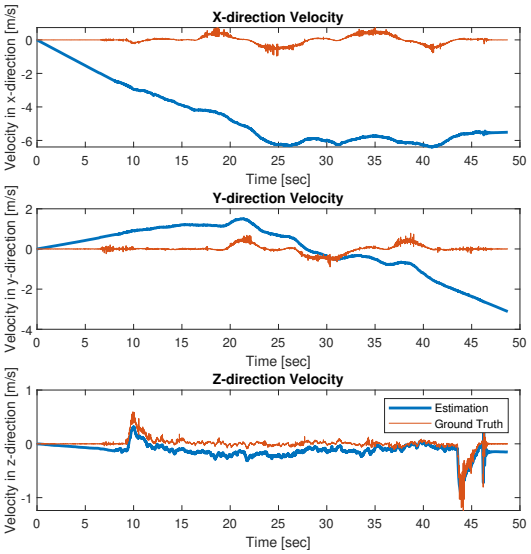

Fig. 3 INS only case velocity estimations.

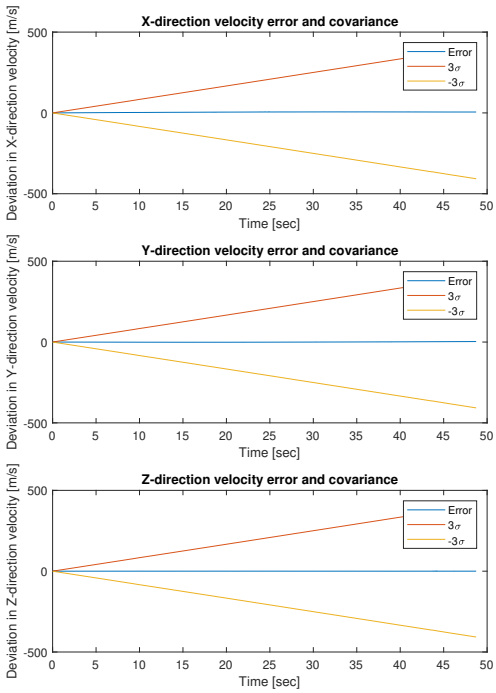

Fig. 4 INS only case velocity estimation covariances.

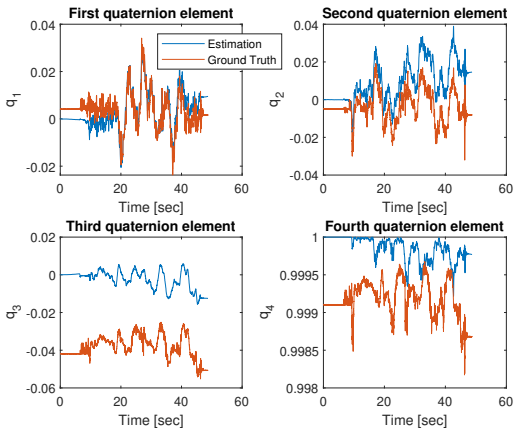

Fig. 5 INS only case quaternion estimations.

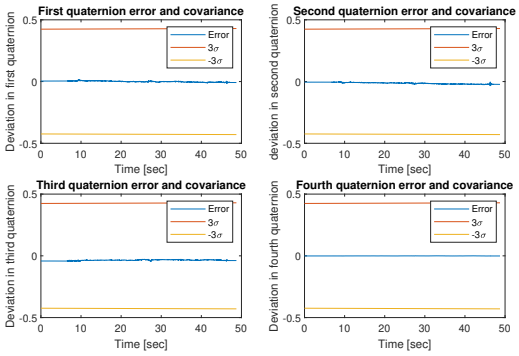

Fig. 6 INS only case quaternion estimation covariances.

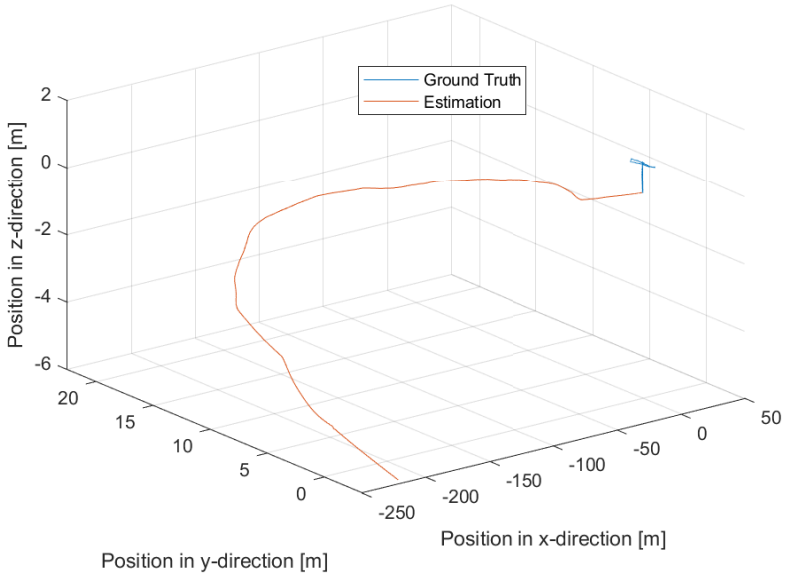

Fig. 7 INS only case 3-D estimation.

From the results, one can see that INS-only navigation is not sufficient. Both position and velocity estimations deviate from the ground truth. Also, the covariances of the position and velocity diverge quite rapidly. The initialization, sensor, and process errors accumulate with time, along with integration. Therefore, external measurement, such as UWB, is needed to find the optimum navigation solution.

Integrated navigation solution of INS and external UWB measurements for a tightly coupled navigation system is presented below in Figures 8 to 14 as follows.

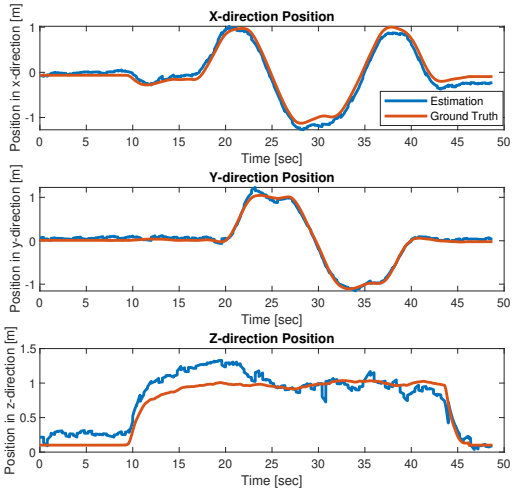

Fig. 8 UWB case position estimations.

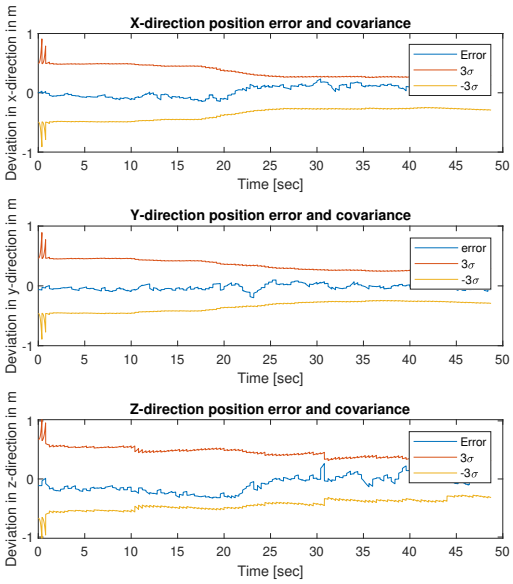

Fig. 9 UWB case position estimation covariances.

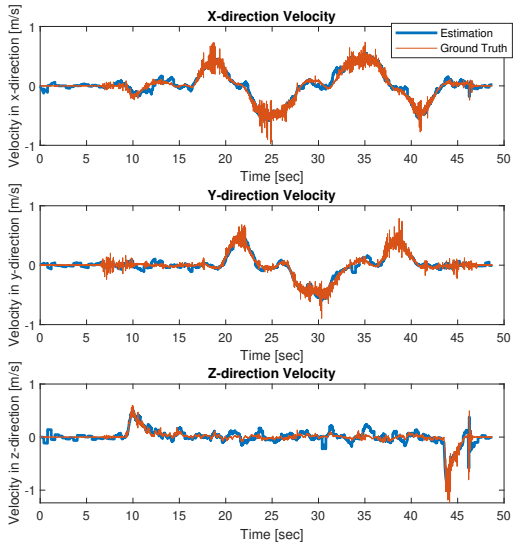

Fig. 10 UWB case velocity estimations.

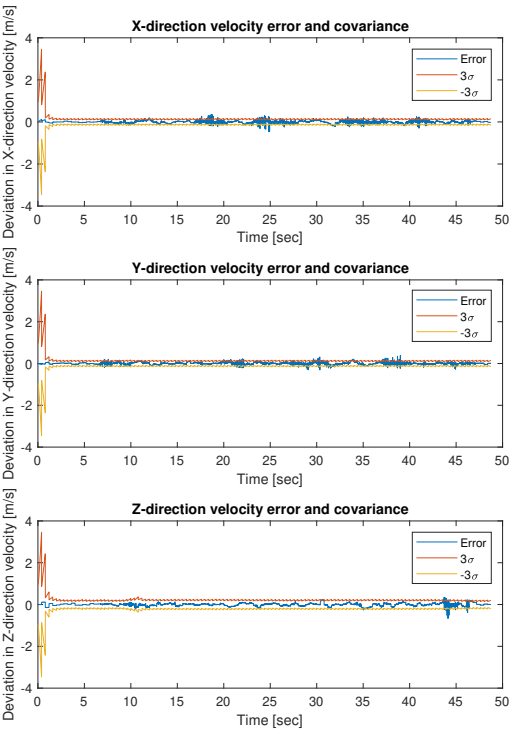

Fig. 11 UWB case velocity estimation covariances.

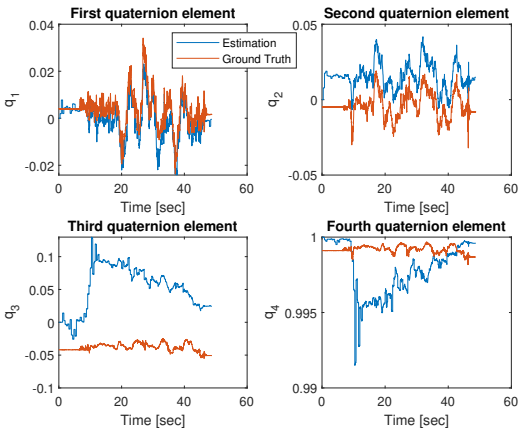

Fig. 12 UWB case quaternion estimations.

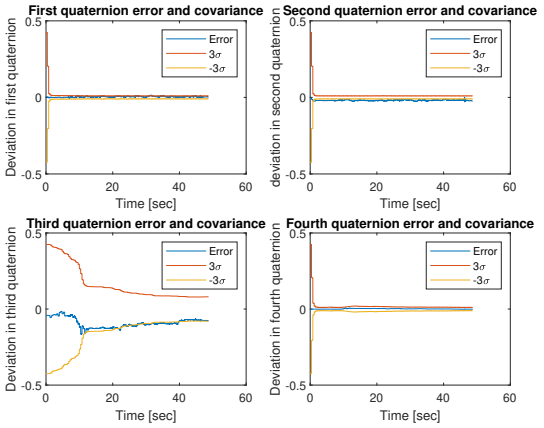

Fig. 13 UWB quaternion estimation covariances.

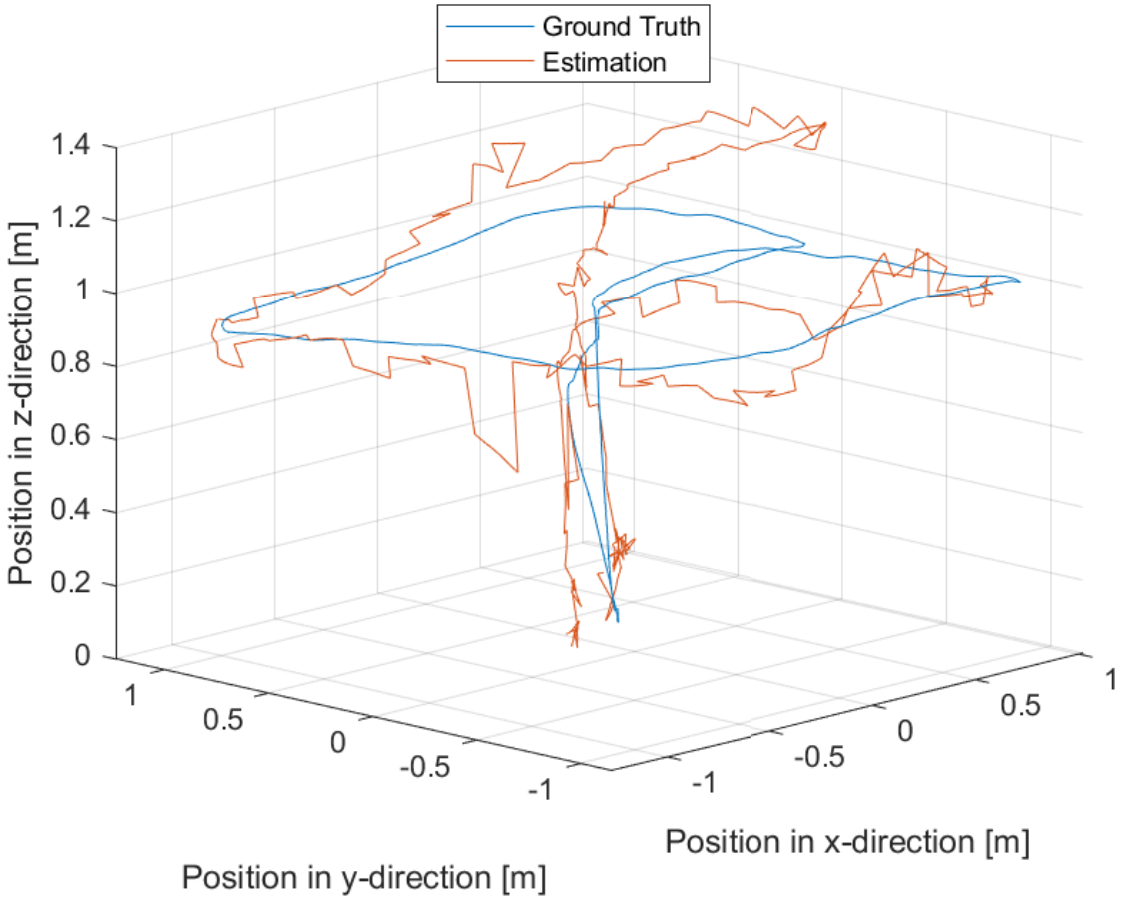

Fig. 14 UWB case 3-D estimation.

For the UWB external measurement case, we can see that the positions and velocities are estimated well. Even though there is bias in the UWB measurements, they are estimated and taken into consideration in the algorithm. However, there is a relatively significant error in the Z-direction position. This is expected due to the GDOP of the UWB anchor's geometry. Also, note that we see noise-like deviations in the ground truth velocity values since they are

not provided and obtained by discretizing the provided position values. From the covariance plots for position and velocity, we can conclude that the EKF works quite well since the covariances converge to the same value with time, and the errors are between the 3σ bounds. Also, we can see constant covariances at the beginning of the simulation, which is due to the fact that the drone is not moving at this time interval, like in the first ten seconds. Regarding the quaternions, since we don't have direct measurement updates and they are mainly estimated by the filter process, there is a relatively significant error seen in the quaternion estimations. Because the mapping between the range measurements and the quaternions is weak, the filter has difficulties in estimating the quaternions properly. Also, we can see that in the quaternion covariance plot, 3σ bounds are exceeded from time to time. Note that due to the constant bias-like errors in the estimation of INS only case in quaternions as illustrated in Figure 5, we have a bias in the gyro measurements, which makes the estimation in the quaternion even harder for our navigation problem.

Therefore, another external measurement can be utilized to estimate the attitude of the drone and, as a result, to have a better navigation solution. The available VIO measurements are utilized and added to the filter along with UWB measurements as a tightly coupled system, and results are given in the following Figures15 to 21.

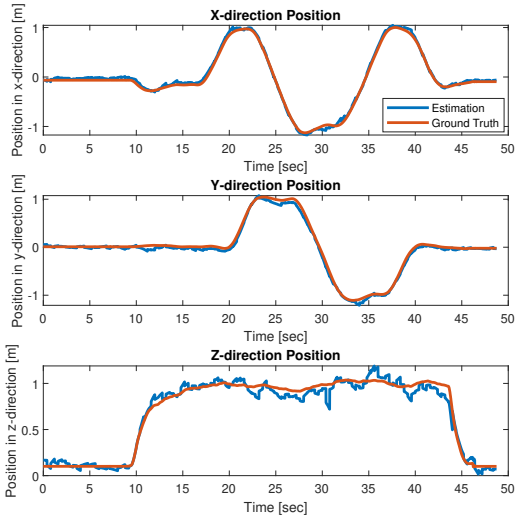

Fig. 15 UWB and VIO case position estimations.

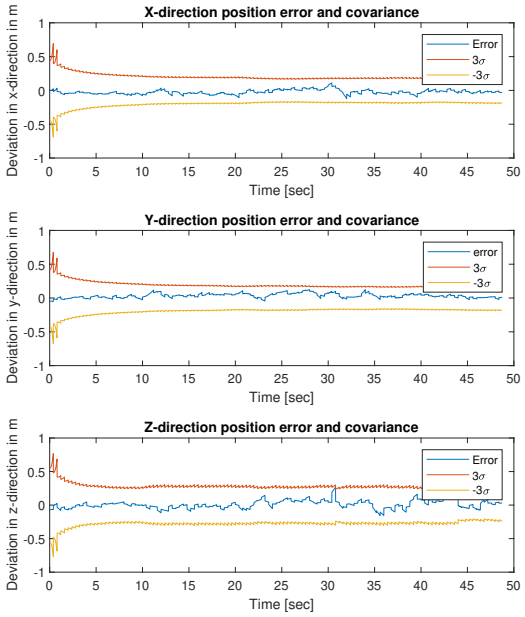

Fig. 16 UWB and VIO case position estimation covariances.

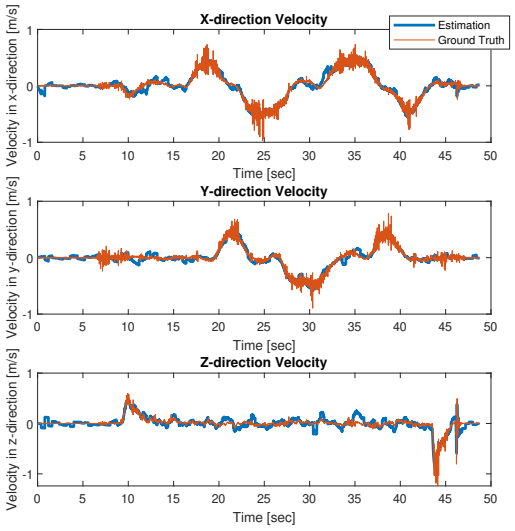

Fig. 17 UWB and VIO case velocity estimations.

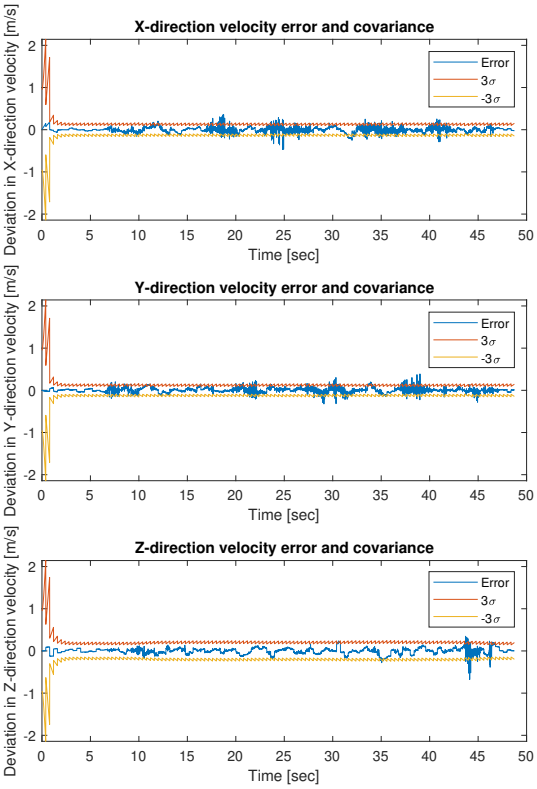

Fig. 18 UWB and VIO case velocity estimation covariances.

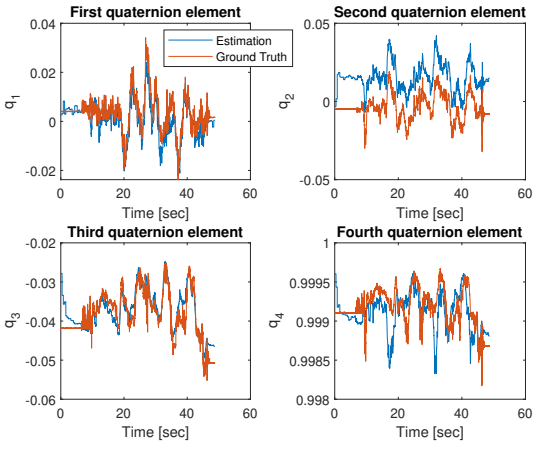

Fig. 19 UWB and VIO case quaternion estimations.

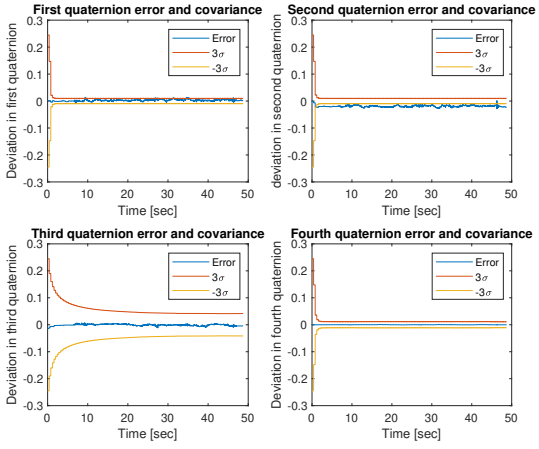

Fig. 20 UWB and VIO quaternion estimation covariances.

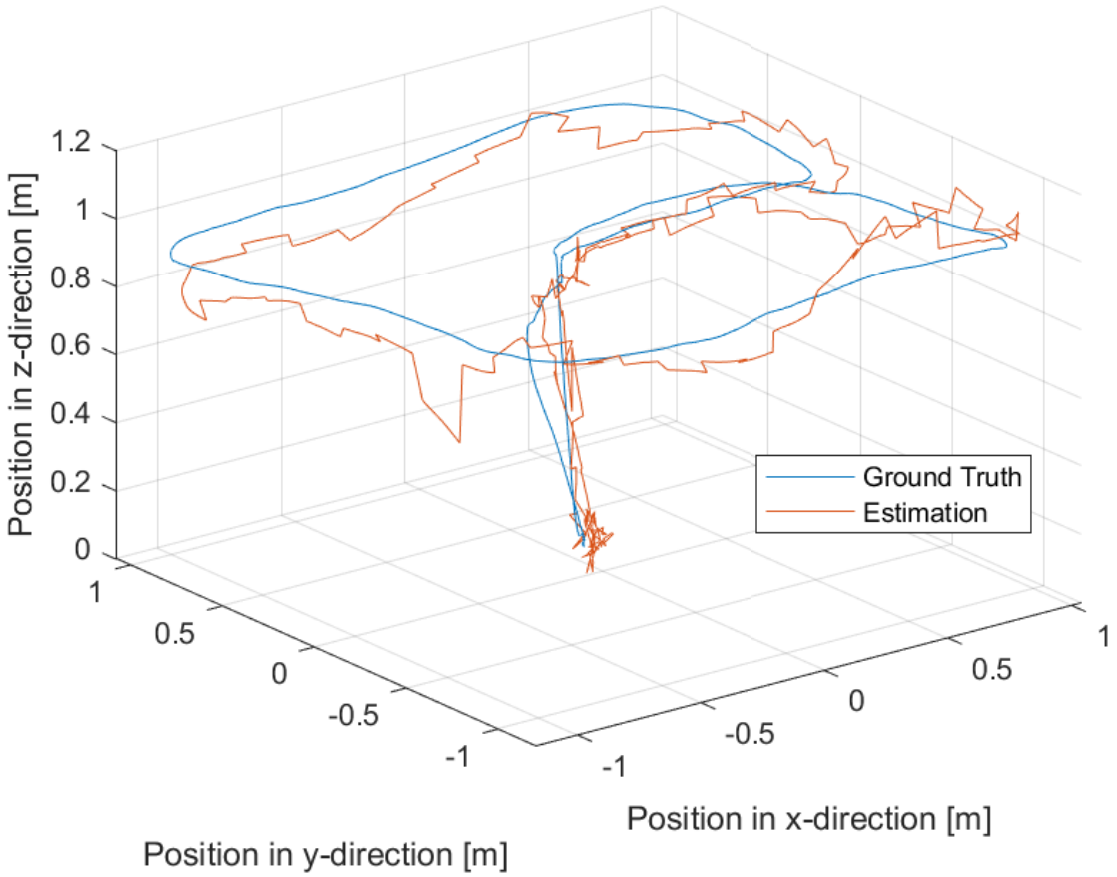

Fig. 21 UWB and VIO case 3-D estimation.

Finally, from the results obtained by UWB and VIO external measurements, we can see that estimation in positions, velocities, and quaternions improved significantly. Note that there were also biases in the VIO measurements, but they are estimated at the beginning of the algorithm for ease from the initial measurements to have calibration in the VIO measurements. Although it is improved compared to the UWB case in the z-axis position estimation, we can see relatively good error compared to the x and y directions, and again, it is expected due to the GDOP of the anchors. The covariance plots, as expected, get smaller with time and converge to some constant value as the EKF progresses. The errors are between the 3σ bounds, which shows that the filter works well. Lastly, we have some constant bias, like an error in the second quaternion that couldn't resolved, and it is assumed to be due to the constant bias that fed into the algorithm that isn't considered. Our best guess is that it is due to the miss alignment of the body axis with the VIO principal axis. In conclusion, the most optimal navigation solution is obtained by UWB - VIO external measurements.

VI. Future Studies

In future work, several improvements will be made to enhance the drone's indoor navigation. The Unscented Kalman Filter will be used instead of the Extended Kalman Filter to better handle aggressive maneuvers and improve accuracy. Also, an error state analysis will be conducted to identify and correct biases in the measurements from UWB and VIO, aiming to fix consistent errors and increase reliability. Finally, these improvements will be compared various indoor settings to ensure their effectiveness and correctness in real-life situations.

VII. Conclusion

In this study, the navigation problem for a drone in the indoor environment is analyzed for real data with different approaches. The best result is obtained via tightly coupled EKF with two different external measurements of UWB and VIO. The results are quite sufficient, but they can be improved by integrating the Unscented Kalman Filter algorithm to have better results in highly nonlinear relations. Also, we can see that the main error comes from the bad estimations of the attitudes, which can be eliminated by estimating the gyro bias more profoundly in error domain implementation to the algorithm instead of the full state.

References

[1] Mueller, T., "On the Birth of Micro Air Vehicles," *International Journal of Micro Air Vehicles*, Vol. 1, 2009, pp. 1–12. https://doi.org/10.1260/1756-8293.1.1.1.

[2] Abderahman Rejeb, S. J. S., Karim Rejeb, and Treiblmaier, H., "Drones for supply chain management and logistics: a review and research agenda," *International Journal of Logistics Research and Applications*, Vol. 26, No. 6, 2023, pp. 708–731. https://doi.org/10.1080/13675567.2021.1981273.

[3] Lab, U. D. S., "Range-Aided Localization," , 2024. URL https://utiasdsl.github.io/utias_ra_loc/01_range_aided_localization.html, accessed: 2024-06-23.

[4] Goudar, A., and Schoellig, A. P., "Online spatio-temporal calibration of tightly-coupled ultrawideband-aided inertial localization," *2021 IEEE/RSJ International Conference on Intelligent Robots and Systems (IROS)*, IEEE, 2021, pp. 1161–1168.

[5] Guo, K., Qiu, Z., Miao, C., Zaini, A. H., Chen, C.-L., Meng, W., and Xie, L., "Ultra-wideband-based localization for quadcopter navigation," *Unmanned Systems*, Vol. 4, No. 01, 2016, pp. 23–34.

[6] Mueller, M. W., Hamer, M., and D'Andrea, R., "Fusing ultra-wideband range measurements with accelerometers and rate gyroscopes for quadrocopter state estimation," *2015 IEEE International Conference on Robotics and Automation (ICRA)*, IEEE, 2015, pp. 1730–1736.

[7] Prorok, A., Gonon, L., and Martinoli, A., "Online model estimation of ultra-wideband TDOA measurements for mobile robot localization," *2012 IEEE International Conference on Robotics and Automation*, Ieee, 2012, pp. 807–814.

[8] Kaufmann, E., Bauersfeld, L., Loquercio, A., Müller, M., Koltun, V., and Scaramuzza, D., "Champion-level drone racing using deep reinforcement learning," *Nature*, Vol. 620, No. 7976, 2023, pp. 982–987.

[9] Webb, T. P., Prazenica, R. J., Kurdila, A. J., and Lind, R., "Vision-based state estimation for autonomous micro air vehicles," *Journal of guidance, control, and dynamics*, Vol. 30, No. 3, 2007, pp. 816–826.